THE JOURNAL OF PHYSICAL CHEMISTRY C

Article

Cite This: J. Phys. Chem. C 2019, 123, 7810−7817

pubs.acs.org/JPCC

Electron Binding Energy Spectra of Al_nMo^- Clusters: Measurements, Calculations, and Theoretical Analysis

Paulo H. Acioli,[†] Xinxing Zhang,[‡] Kit H. Bowen, Jr.,[*,§] and Julius Jellinek[*,∥]

[†]Department of Physics, Northeastern Illinois University, Chicago, Illinois 60625, United States

[‡]Collaborative Innovation Center of Chemical Sciences and Engineering, College of Chemistry, Nankai University, Tianjin 300071, China

[§]Departments of Chemistry and Materials Science, Johns Hopkins University, Baltimore, Maryland 21218, United States

[∥]Chemical Sciences and Engineering Division, Argonne National Laboratory, Argonne, Illinois 60349, United States

Supporting Information

ABSTRACT: Results of photoelectron spectroscopy measurements and density functional theory complemented with correction scheme calculations on electron binding energy (EBE) spectra of anionic Al_nMo, n = 3−5 and 7, clusters are presented and analyzed. The analysis points to the important role of dynamical fluxionality and multiplicity of structural forms as contributing factors in the measured spectra. Using the example of Al_4Mo^- as a paradigmatic case, the separate roles of size, structure/symmetry, and composition in evolving the EBE spectra of precursor pure clusters (in this case, Al_4^- and Al_5^-) into those of bimetallic clusters are demonstrated utilizing a new methodology we developed recently (*J. Phys. Chem. C* **2017**, *121*, 16665).

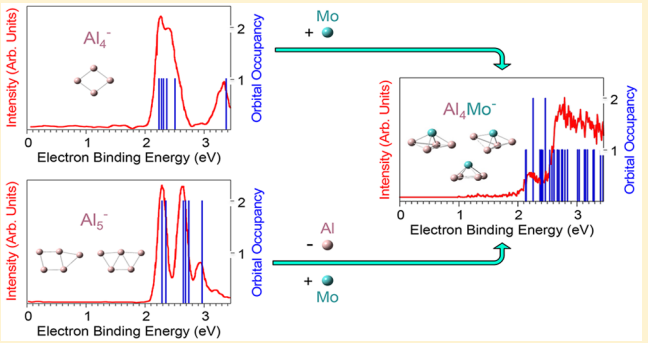

INTRODUCTION

Clusters of metallic elements continue to be the subject of intense fundamental research, both experimental and theoretical/computational (see, e.g., refs 1 and 2 and citations therein). The interest in them is fueled by the remarkable variety of all their properties—structural, electronic, magnetic, optical, chemical and others—and the dramatic changes in these properties as a function of cluster size. Their small- and medium-size systems are actually not metals from the materials point of view because they are devoid of features characteristic of the bulk metallic state. These features then "grow in" as the clusters grow in size (see, e.g., refs 3−6 and citations therein). The phenomenon of size-induced transition to metallicity remains a fascinating subject. The variety and variability of properties and, consequently, functionalities also impart metal clusters and nanoparticles a central role in new emerging technologies.

A particularly rich area of metal cluster/nanoparticle research is the field of nanoalloys (see, e.g., refs 2 and 7−9 and citations therein) where, in addition to size and structure, another knob—composition—can be used for tuning properties and characteristics. It is not surprising then that in recent years the center of activity in metal cluster/nanoparticle research has shifted to nanoalloys.

Among the techniques and methodologies used in studies of metal clusters, and more generally finite-size systems, photoelectron spectroscopy (PES) emerged as a particularly powerful tool (see, e.g., refs 10 and 11 and citations therein). Photodetached electrons provide information on a broad variety of properties. This is particularly true when PES measurements are combined with theoretical/computational studies (cf. refs 3−5 and 11−15 and citations therein). This combination allows for characterization of: (1) electronic structure and geometric (isomeric) form, or forms, of a system generated under specific experimental conditions; (2) investigation of the changes in the electronic and geometric structure with the size of the system; and (3) exploration, in the case of nanoalloys, of the changes in the electronic structure and conformation (both isomeric and homotopic[16]) of a system caused by adding or substituting some of its atoms by atoms of another element. The majority of the PES studies of metal clusters is still on one-component systems, although the number of experiments on nanoalloys is increasing.[15,17−24] A complicating aspect in the interpretation of results is that all three factors—size, structure/symmetry, and composition—have a simultaneous effect on measured PES data. The function of theoretical/computational studies in this respect is central. As has been demonstrated recently,[15] these studies can provide insight into the separate roles of size, structure/symmetry, and composition, even though they are coupled, in

Special Issue: Hans-Joachim Freund and Joachim Sauer Festschrift

Received: July 15, 2018
Published: August 10, 2018

DOI: 10.1021/acs.jpcc.8b06769
J. Phys. Chem. C 2019, 123, 7810−7817

explaining the differences in measured PES results. These differences are often dramatic even in cases of "neighboring" cluster systems.

In this paper we present the results of a combined experimental/theoretical study on the EBE spectra of Al_nMo^-, n = 3−5 and 7. The methodological details are outlined in the next section. These are followed by the results of our measurements and calculations and their analysis. A brief summary is given in the conclusion.

METHODOLOGICAL DETAILS

Experimental. Our PES apparatus consists of a pulsed arc cluster ionization source (PACIS), a time-of-flight mass spectrometer, a Nd:YAG photodetachment laser, and a magnetic bottle electron energy analyzer with a resolution of ∼35 meV at 1 eV electron kinetic energy (EKE); the details can be found in refs 25 and 26. The known atomic transitions in Cu^-[27] were used for calibration of the photoelectron spectra.

The Al_nMo^- cluster ions were generated in the PACIS. In this source, a strong current is discharged through a sample, which in our case was a mixture of aluminum and molybdenum powders pressed onto an Al rod. The carrier gas was helium, which was supplied by a pulsed gas valve behind the discharge region. The carrier gas cools down the initially hot clusters, but their temperature is difficult to evaluate. We roughly estimate it to be ∼150 K above room temperature.

The PES measurements were performed by crossing a beam of mass-selected Al_nMo^-, n = 3−5 and 7, with a fixed-frequency photon beam and energy analyzing the photodetached electrons. The photon energy was 3.49 eV. The EBEs were obtained from the energy balance equation

$$h\nu = \mathrm{EBE} + \mathrm{EKE} \quad (1)$$

where $h\nu$ is the photon energy.

Theoretical/Computational. The calculations were performed within the gradient-corrected density functional theory (DFT) with the Becke exchange[28] and Perdew correlation[29] functionals (BP86) and the Stuttgart pseudopotentials/basis sets[30] for Al and Mo as implemented in the Gaussian 03 package.[31] The choice of BP86 was based on tests that included the BPW91 and PBE functionals as alternatives and evaluated the calculated properties of the Al and Mo atoms as well as Al_2 and Mo_2 dimers against the available experimental data (see Table S1 in the Supporting Information). The restricted and unrestricted formalisms were used in cases with, respectively, even an odd number of electrons.

The DFT framework was complemented by a correction scheme[32] to obtain the true electron eigenenergies E_i and electron binding energies EBE_i from the nonphysical Kohn−Sham eigenenergies ε_i, where i labels the orbitals/electrons. The scheme is rigorous in that it uses only data obtained within DFT as a ground state theory, and it yields orbital-specific corrections Δ_i. The knowledge of the latter allows for determination of the EBE_i and E_i values using the equation

$$\mathrm{EBE}_i = -E_i = -\varepsilon_i + \Delta_i \quad (2)$$

Low-energy equilibrium configurations of the clusters were obtained through gradient-based optimization with no symmetry constraints imposed. A large number of initial guess structures were used, and various spin states were considered. In the case of bimetallic Al_nMo^-, different locations of Mo within a given geometric (isomeric) form were considered, and the energetically most preferred ones were determined. The binding energies $E^b_{\mathrm{Al}_n\mathrm{Mo}^-/\mathrm{Al}_{n+1}^-}$ of the mixed Al/Mo and pure Al cluster anions were calculated as

$$E^b_{\mathrm{Al}_n\mathrm{Mo}^-/\mathrm{Al}_{n+1}^-} = (n)E_{\mathrm{Al}} + E_{\mathrm{Mo}^-/\mathrm{Al}^-} - E_{\mathrm{Al}_n\mathrm{Mo}^-/\mathrm{Al}_{n+1}^-} \quad (3)$$

where E_{Al}, $E_{\mathrm{Mo}^-/\mathrm{Al}^-}$, and $E_{\mathrm{Al}_n\mathrm{Mo}^-/\mathrm{Al}_{n+1}^-}$ are the energies of the Al atom, Mo^- or Al^- anion, and Al_nMo^- or Al_{n+1}^- cluster, respectively (in the case of mixed Al/Mo anions the extra electron was associated with the Mo atom because its electron affinity is higher than that of the Al atom—see Table S1).

The values of the calculated Kohn−Sham eigenenergies and correction terms together with the corresponding electron binding energies obtained using eq 2 are listed for the lowest energy structures of Al_nMo^-, n = 3−5 and 7, and Al_n^-, n = 4 and 5, as well as Mo and Al atoms (these are the systems analyzed in detail in the next section) in Tables S2−S9. Inspection of the correction terms indicates that in general they are different in different systems, and within each system they are orbital-dependent. The degree of orbital dependence, however, decreases as the size of the systems increases. For that reason, the EBE_i and E_i values of Al_3Mo^-, Mo, Al, and Al_4^- we present and analyze in the next section were calculated with the actual orbital-specific corrections (cf. Tables S2 and S6−S8). For Al_nMo^-, n = 4, 5, and 7, and Al_5^- a constant correction term equal to that for the system's corresponding HOMO level was applied to all the Kohn−Sham eigenenergies (cf. Tables S3−S5 and S9). These recipes were employed for all the structures (not only the lowest energy ones) used in the analysis (see below).

RESULTS AND DISCUSSION

Figure 1 shows low-energy equilibrium configurations of Al_nMo^-, n = 3−5 and 7, and their characteristics as obtained in our calculations. For each cluster size, the figure displays the corresponding most stable structure, and if available, additional stationary conformations whose energies ΔE referred to that of the most stable structure fall within the room-temperature vibrational energy gap of $(3m - 6)kT$, where $m = n + 1$ is the number of atoms in the cluster, k is the Boltzmann constant, and T = 300 K (see Tables S10 and S11). We found 2, 1, and 5 such additional conformations for Al_4Mo^-, Al_5Mo^-, and Al_7Mo^-, respectively. Even though the temperature of the experiment was higher than room temperature, the sets of structures in Figure 1 for the different cluster sizes fully account for all the features in the corresponding measured PES graphs (see below).

The case of Al_4Mo^- is particularly interesting. One of the additional conformations is another minimum energy structure that is only 0.055 eV higher in energy than the most stable one and has the same symmetry and spin as the latter. The two, however, correspond to different electronic states: $^2A_1$ for the most stable structure and $^2B_2$ for the higher energy configuration. The second additional conformation is a transition state (TS) geometry with C_{4v} symmetry whose energy is only 0.010 eV higher than that of the $^2A_1$ state structure. This TS connects the $^2A_1$ structure with another one that is geometrically and electronically equivalent to it. The additional conformations for Al_5Mo^- and Al_7Mo^- are all minimum energy configurations. A common element in all the structures of Figure 1 is that the Mo atom occupies a high coordination site.

DOI: 10.1021/acs.jpcc.8b06769
J. Phys. Chem. C 2019, 123, 7810−7817

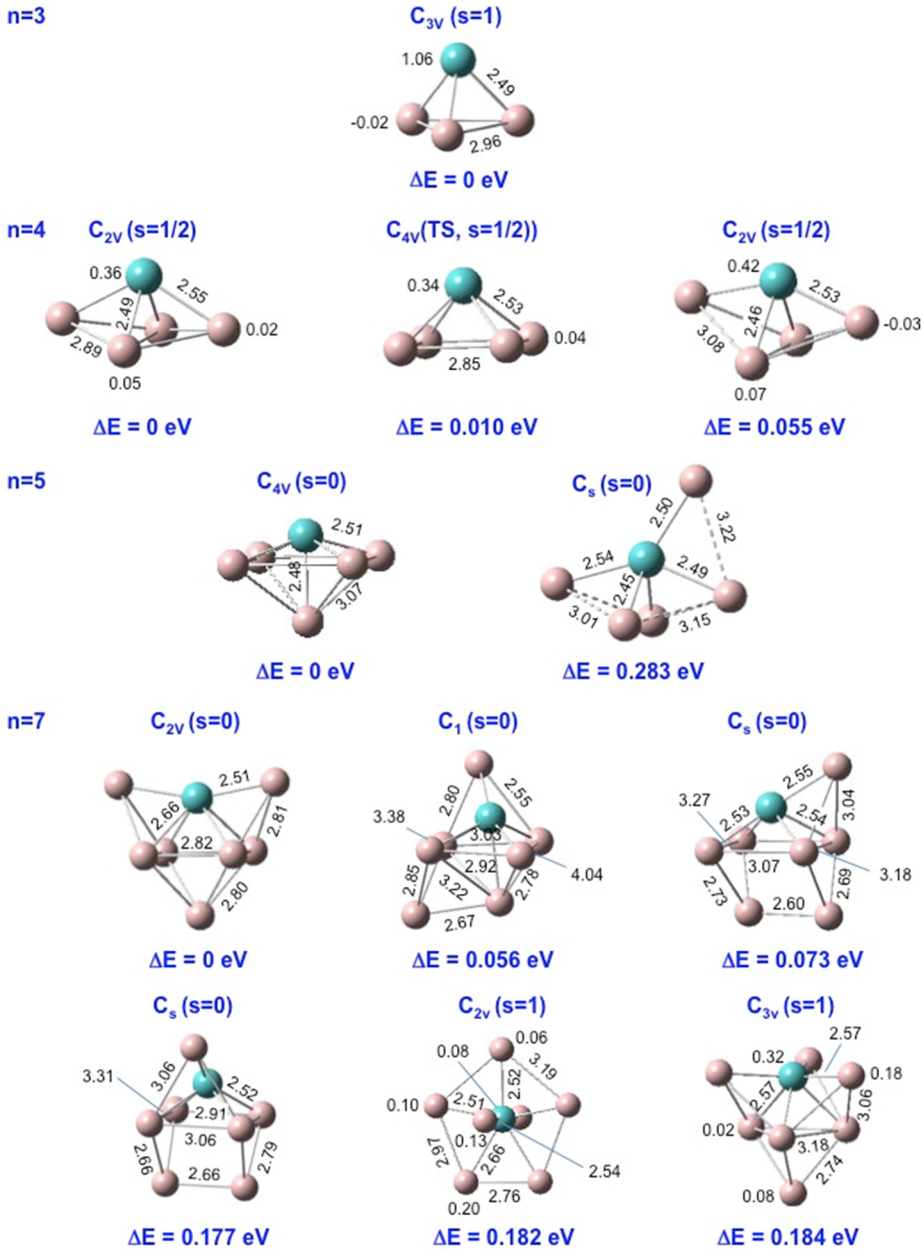

Figure 1. Optimized low-energy structures of Al_nMo^-, n = 3−5 and 7 (Mo is shown in blue). Indicated are the energies ΔE in eV referred to the energy of the corresponding most stable structure, the symmetry, the total spin s, the interatomic distances in Å, and, except when zero, the individual atomic spins. TS denotes a transition state configuration.

Figures 2−5 display the measured PES graphs and the corresponding calculated structure-specific EBE spectra. For all cases, the calculated EBEs fall under the experimental graphs, and the two also display a good qualitative agreement. The accuracy of the calculated EBEs obtained with the corrections as indicated above is estimated to be within about ±0.1 eV. This estimate follows from the analysis of the calculated vs measured data, especially for the electron affinities, presented in Table S1, and the differences between the orbital-specific and constant corrections in Tables S3−S5 and S9.

The figures indicate that, with the exception of the case of Al_3Mo^-, the measured PES graphs incorporate contributions from multiple structures depicted in Figure 1. Consider, for example, the case of Al_4Mo^-. As is clear from Figure 3, invoking the higher energy $^2B_2$ state structure, in addition to the most stable $^2A_1$ state conformation, is essential for understanding the measured PES graph, especially its segment between ∼2.8 eV and ∼3.3 eV. In addition, because the barrier between the equivalent forms of the $^2A_1$ conformation is smaller than the zero-point energy of the latter (this remains true if one takes into account the zero-point energy of the TS as well but also adds, even if only, the room-temperature thermal energy (see Tables S10 and S11)), it is fluxional and undergoes constant interconversion between its equivalent forms. This interconversion is further helped by extra thermal energy. The configurations traced out in the course of the interconversion, including that of the TS, also contribute to the measured spectrum. The bottom panel of Figure 3 displays the EBEs calculated for the TS configuration.

The barrier height for conversion of the $^2B_2$ structure into its equivalent is high. However, the crossing point between the $^2A_1$ and $^2B_2$ electronic configurations of the cluster is just 0.060

DOI: 10.1021/acs.jpcc.8b06769
J. Phys. Chem. C 2019, 123, 7810−7817

eV above the equilibrium energy of the $^2A_1$ structure (see Figure S1 in the Supporting Information), and consequently the two C_{2v} structures with different electronic configurations also undergo interconversion. All these factors play a role in defining the shape of the measured PES spectrum of Al_4Mo^-. In the cases of Al_5Mo^- (Figure 4) and Al_7Mo^- (Figure 5), the number of minimum energy conformations that contribute to the measured PES graph is two and six, respectively.

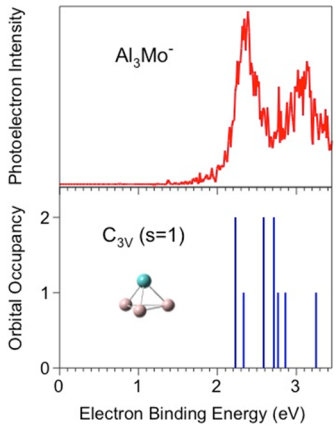

Figure 2. Measured (continuous graph) and calculated (vertical bars) electron binding energy spectra of Al_3Mo^-. The calculated results are for the most stable form of the cluster whose structure, symmetry, and total spin *s* are also shown.

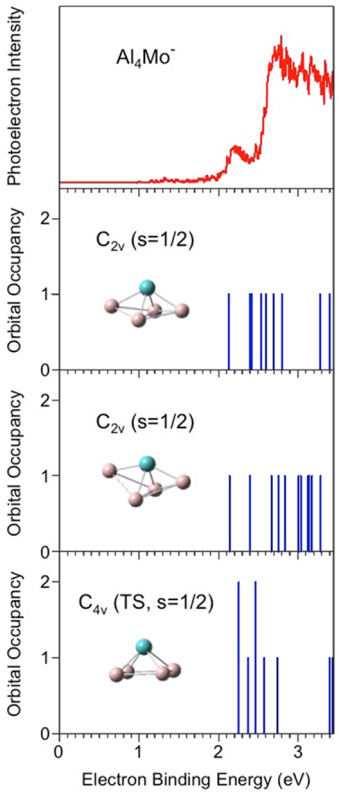

Figure 3. Same as Figure 2, but for Al_4Mo^-. The calculated results are shown not only for the most stable structure but also for other low-energy conformations of the cluster. See the text for details.

An important aspect of analysis and interpretation of experimental cluster PES data is their "genesis", that is, their

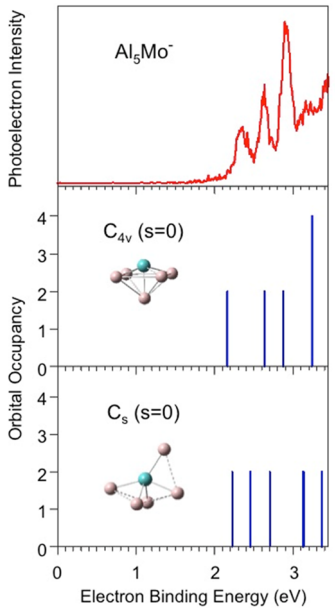

Figure 4. Same as Figure 3, but for Al_5Mo^-.

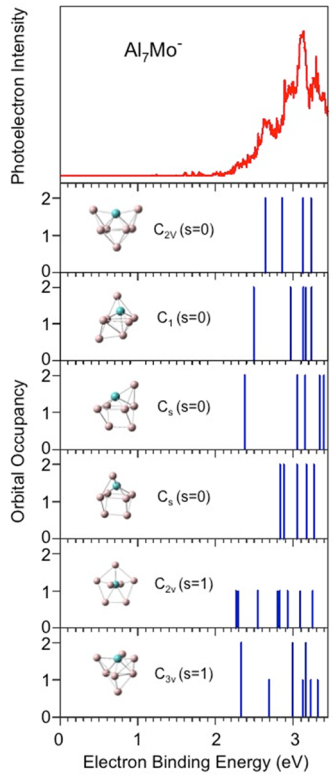

Figure 5. Same as Figure 3, but for Al_7Mo^-.

dependence on factors such as size, structure, and composition. The task is to elucidate the separate role of each of these factors even when they all are involved simultaneously. Recently, we formulated a general methodology for accomplishing this task.[15] Here we apply it to establish the genesis of the spectrum of the Al_4Mo^- cluster. The latter can be obtained from pure anionic Al clusters by adding a Mo atom to Al_4^- or substituting an Al atom by a Mo atom in Al_5^-.

Figure 6 reproduces parts of earlier measured PES data[33] (reproduced with permission) for Al_4^- and Al_5^- (cf. also ref

DOI: 10.1021/acs.jpcc.8b06769
J. Phys. Chem. C 2019, 123, 7810−7817

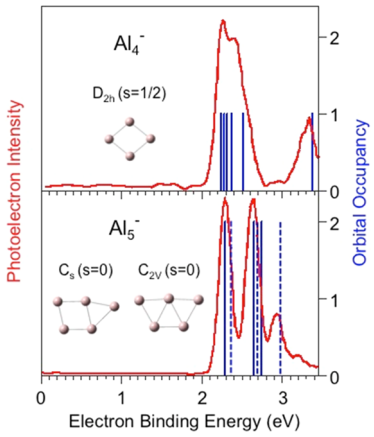

Figure 6. Measured (continuous graphs, reproduced with permission from ref 33) and calculated (vertical bars) electron binding energy spectra of Al_4^- and Al_5^-. The calculated spectra are for the lowest energy structures of the clusters (solid bars) and, in the case of Al_5^-, also for the C_{2v} TS configuration (dashed bars). See the text for details.

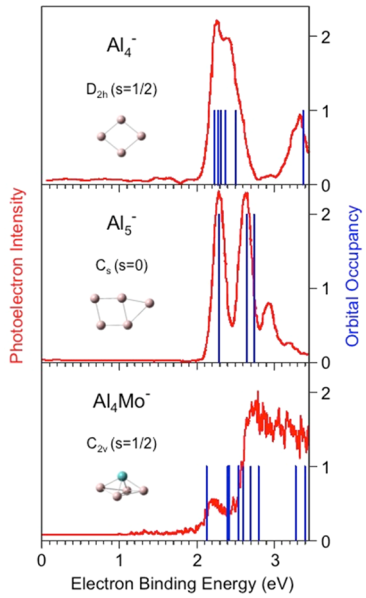

Figure 7. Measured (continuous graphs) and calculated (vertical bars) electron binding energy spectra of Al_4^-, Al_5^-, and Al_4Mo^-. The measured graphs for Al_4^- and Al_5^- are reproduced with permission from ref 33. The calculated spectra are for the lowest energy structures of the clusters.

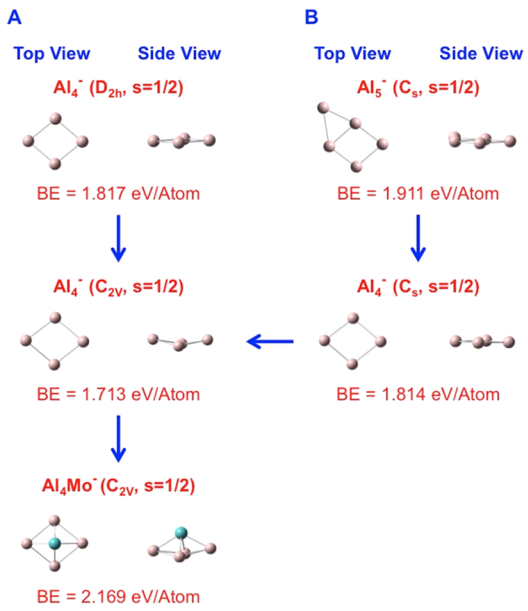

Figure 8. Schematics of the step-by-step conversion of Al_4^- (panel A) and Al_5^- (panels B and A) into Al_4Mo^-. See the text for details.

34). The figure also shows the structure-specific EBEs of these clusters obtained in our present calculations. As clearly seen in the figure, the calculated EBE spectrum of the most stable D_{2h} structure of Al_4^- alone fully accounts for all the features in the graph of the measured data. That is not the case for Al_5^-: its lowest energy planar C_s structure does not explain the third peak in the experimental graph. It turns out, however, that this C_s structure is separated from another C_s structure that is geometrically and electronically equivalent to it by an energy barrier of just 0.027 eV. As a consequence, similarly to the case of Al_4Mo^- discussed above, Al_5^- undergoes constant interconversion from one C_s structure to another and back, and that interconversion takes place via a TS that has C_{2v} symmetry (also shown in the figure). The importance of taking into account the contribution of the TS is transparent: it is responsible for the third peak in the experimental graph. It also explains why the third peak is a minor one: the first two peaks get contributions from both the most stable structure and the TS conformation.

We turn now to the analysis of how the PES graphs of Al_4^- and Al_5^- evolve into that of Al_4Mo^- upon addition and substitution, respectively, of a Mo atom. For convenience we display the three graphs together in Figure 7. It is clear that they are very different. The graph of Al_4^- contains a peak with a shoulder followed by a second peak. The graph of Al_5^- contains, as already mentioned, two distinct major peaks followed by a third minor peak. Finally, the graph of Al_4Mo^- displays a first minor peak that is followed by a very broad major second peak; the latter may be a result of an overlap of many narrower peaks. The analysis of the evolution of the graphs of Al_4^- and Al_5^- into that of Al_4Mo^- is performed below in terms of segments/contributions associated with the corresponding lowest energy structures of the clusters; the calculated EBE spectra of these are also shown in Figure 7.

The schematics of the step-by-step conversion of the most stable forms of Al_4^- and Al_5^- into that of Al_4Mo^- are shown in, respectively, panels A and B of Figure 8. The first step in the conversion of Al_4^- is to transform it from its most preferred planar structure with D_{2h} symmetry into a three-dimensional structure with a boat shape and C_{2v} symmetry that is "conditioned" to accept the Mo atom; the conditioned structure of Al_4^- is obtained from the most stable C_{2v} structure of Al_4Mo^- by removing the Mo atom. Next, the Mo atom is added to the conditioned Al_4^- to form Al_4Mo^-. The spectra of the electron eigenenergies E_i calculated for the species involved in these steps and the correlations between them are shown in Figure 9. Apart from symmetry, the correlations are based on the examination of the orbital character of the corresponding one-electron levels. The boxes indicate groups of E_i's that underlie, or are precursors to, the peaks in the corresponding experimental graphs.

As seen in Figure 9, the effect of conditioning Al_4^-, which is a structure/symmetry effect, is to shift the E_i's that underlie the

DOI: 10.1021/acs.jpcc.8b06769
J. Phys. Chem. C 2019, 123, 7810−7817

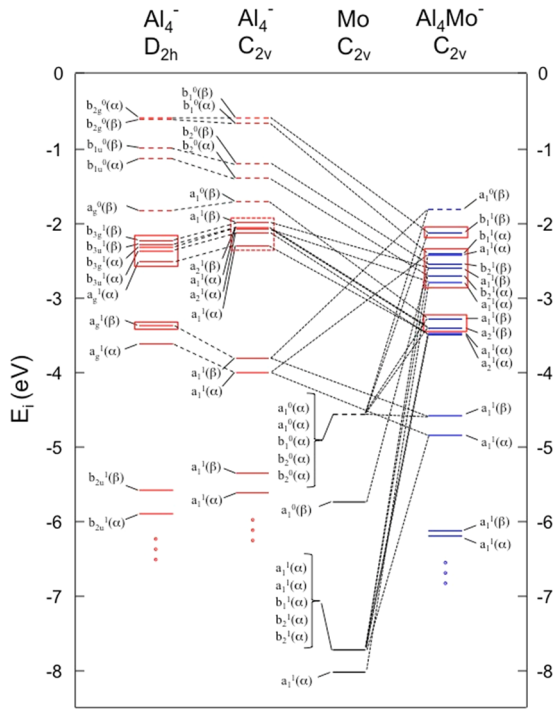

Figure 9. Electron eigenenergy E_i spectra and the correlations between them for the lowest energy D_{2h} structure of Al_4^-, the conditioned C_{2v} form of Al_4^-, the Mo atom under the C_{2v} symmetry, and the lowest energy C_{2v} conformation of Al_4Mo^-. The boxes indicate groups of eigenenergies that underlie (solid-line boxes) or are precursors of (dashed-line boxes) the peaks in the measured PES graphs. See the text for details.

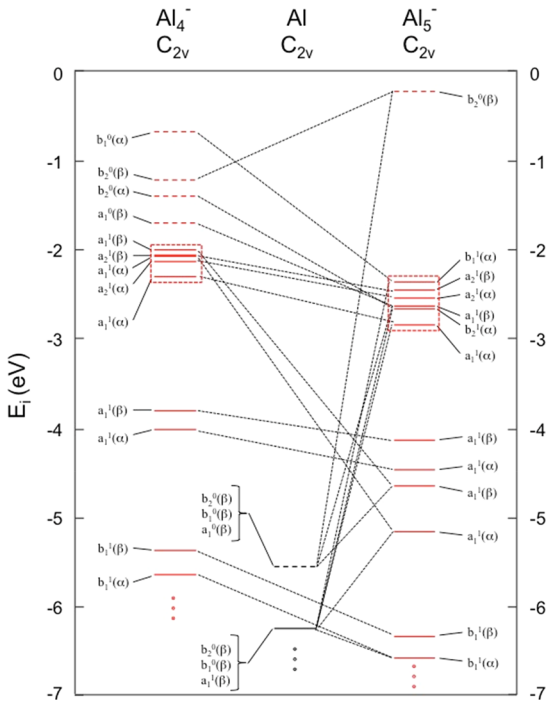

Figure 10. Same as Figure 9, but for the conditioned C_{2v} form of Al_4^-, the Al atom under C_{2v} symmetry, and the conditioned C_{2v} conformation of Al_5^-. See the text for details.

first peak with a shoulder in the experimental graph of Al_4^- to somewhat higher values (or, equivalently, lower EBEs). The accompanying change in the E_i that underlies the second peak in the experimental graph is a somewhat larger in magnitude shift to a lower value (i.e., a higher EBE). The addition of a Mo atom to the conditioned Al_4^- brings 6 extra valence electrons in a $4d^55s^1$ configuration. The consequence of this addition is a substantial reordering of the orbitals. Unoccupied levels of the conditioned Al_4^- shift significantly downward, whereas those of the Mo atom shift upward. They mix and become populated in Al_4Mo^-. The net outcome of this major orbital reordering is that the high spin $s = 3$ of the Mo atom becomes "diluted" in Al_4Mo^- whose spin is $s = 1$. In terms of eigenenergy groupings, the reordering results in three groups of E_i's. The first one underlies the first minor peak in the experimental graph of Al_4Mo^-; the second contributes to the first peak and the lower energy segment of the second broad peak; and the third one is a contributor to the high energy end of the second peak.

The addition of Mo to the conditioned Al_4^- involves a change in both the size and the composition of the cluster. To identify the separate roles of these in forming the pattern of the E_i eigenenergies of Al_4Mo^-, we substituted in the latter the Mo atom by an Al atom, keeping the structure of the cluster intact, and calculated the E_i spectrum of the thus formed conditioned C_{2v} Al_5^- (the substitution reduces the total number of electrons by 29 and the number of valence electrons by 3). The genesis of this spectrum can be understood as originating from the E_i spectrum of the conditioned C_{2v} Al_4^- and subjected to the size effect accompanying the conversion of the C_{2v} Al_4^- into the C_{2v} Al_5^-. As illustrated in Figure 10, the principal consequences of this size effect are a significant shift of some of the unoccupied levels of the conditioned Al_4^- downward and mixing with the HOMO of the added Al atom that splits and shifts upward, and an accompanying split and shift upward of the LUMO of the Al atom that partially mixes with the populated levels of the conditioned Al_4^-. The net result in terms of eigenenergy groupings in the C_{2v} Al_5^- is a broad box of levels that span essentially the same energy range as the levels of the second box in the E_i spectrum of Al_4Mo^- (cf. Figure 9). The first and the third boxes in the spectrum of Al_4Mo^- are missing altogether in the spectrum of the C_{2v} Al_5^-. The levels of these boxes in the spectrum of Al_4Mo^- are consequences of the composition effect—replacement of Al by Mo in the C_{2v} Al_5^-.

The pathway of the stepwise conversion of the most stable C_s form of Al_5^- into the most stable C_{2v} form of Al_4Mo^- is depicted in panel B, in conjunction with panel A, of Figure 8. The first step is to remove an atom from Al_5^-. The atom that is removed is the one that leaves behind an Al_4^- in a C_s structure that is only slightly different from the lowest energy D_{2h} structure of the cluster (it is a neutral Al that is removed because its electron affinity is lower than that of the resulting Al_4; cf. Table S1 and Figure 11). In the second step, the C_s Al_4^- is converted into the conditioned C_{2v} Al_4^-. The final third step is to add a Mo atom to the conditioned Al_4^-.

The correlation diagram that corresponds to the first two steps is shown in Figure 11. As seen in the figure, the effect of the first step, which is a size effect, is to split and change the order of the levels belonging to the two boxes that underlie the first two peaks in the experimental graph of Al_5^- and bring them closer to each other so that they can be viewed as forming a single box in the C_s Al_4^-. Simultaneously, the doubly degenerate a' LUMO level of Al_5^- splits, shifts downward, and gets admixed with the populated levels. The deeper lying doubly degenerate a' level of Al_5^- splits and shifts upward in the C_s Al_4^-. Overall, the E_i spectrum of the latter is very similar

DOI: 10.1021/acs.jpcc.8b06769
J. Phys. Chem. C 2019, 123, 7810−7817

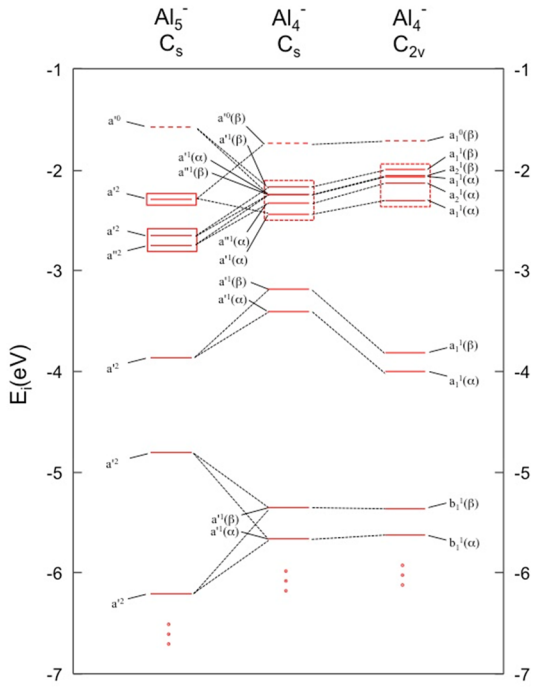

Figure 11. Same as Figure 9, but for the most stable C_s structure of Al_5^-, the intermediate C_s form of Al_4^-, and the conditioned C_{2v} conformation of Al_4^-. See the text for details.

to that of the most stable D_{2h} form of the cluster (cf. Figures 7 and 9). The effect of the second step, which is a structure/symmetry effect, is to shift the top group of populated E_i's slightly upward and spread it a bit. The deeper lying pair of a' levels with different spins shifts significantly downward as they migrate from the C_s Al_4^- to the C_{2v} Al_4^-. Finally, the effects of the third step are depicted in Figure 10 and are analyzed above. [An alternative pathway from Al_5^- to Al_4Mo^- is first to convert the former from its most stable C_s form to its conditioned C_{2v} conformation discussed above and then replace in it the apex Al atom by a Mo atom. The reader is invited to follow the effects of these two steps (structure/symmetry effect and composition effect, respectively) using the data depicted in Figures 9–11.] As mentioned, the preceding analysis is performed in terms of the most stable structures of the clusters. Similar analyses can be performed for all the structures that contribute to the experimental PES graphs.

SUMMARY

In this paper, we presented results of measurements and calculations on EBE spectra of Al_nMo^-, n = 3–5 and 7, clusters and their theoretical analysis. The experiment and calculations are in good accord with each other. The analysis shows that whereas in some cases (e.g., Al_3Mo^-) the size- and composition-dependent features in the graphs of the measured PES data can be explained in terms of the single most stable form of the cluster, in others (as in Al_4Mo^-, Al_5Mo^-, and Al_7Mo^-) they originate from multiple structural forms that may be present in the beam under the experimental conditions. In addition, dynamical fluxionality due to the zero-point vibration, which exhibits itself as an ongoing interconversion between geometrically and electronically equivalent forms of a cluster via a low-energy TS conformation that connects them, may play a role as well (as in Al_4Mo^- and its precursor Al_5^-). The role of the fluxionality is further enhanced by thermal effects.

We also presented an analysis of the genesis of the EBE spectrum of the bimetallic Al_4Mo^- considering it as a paradigmatic case. Specifically, we characterized the separate roles size, structure/symmetry, and composition play in evolving the spectra of the precursor pure Al_4^- and Al_5^- clusters into that of Al_4Mo^- as the former two are converted into the latter through addition and substitution, respectively, of a Mo atom. The knowledge of the separate effects of each of these factors, even though they act simultaneously, and the ability to predict them through calculations will play an ever more important role as our control over nanoscale synthesis increases. They will become indeed indispensable as Feynman's anticipation of being able to "arrange the atoms [one might add, the desired type and number of atoms] one by one the way we want them"[35] gets closer to practical reality.

ASSOCIATED CONTENT

Supporting Information

The Supporting Information is available free of charge on the ACS Publications website at DOI: 10.1021/acs.jpcc.8b06769.

Results of tests of the computational framework; Kohn–Sham eigenenergies and their corresponding correction terms and electron binding energies for the lowest energy structures of Al_nMo^-, n = 3–5 and 7, the Mo and Al atoms, and the lowest energy structures of Al_n^-, n = 4 and 5; normal-mode frequencies, harmonic zero-point energies, and room-temperature thermal energies for the lowest energy structures of Al_nMo^-, n = 3–5 and 7 and the transition state configurations of Al_4Mo^- and Al_5^-; and crossing of two electronic states of the Al_4Mo^- cluster (PDF)

AUTHOR INFORMATION

Corresponding Authors

*E-mail: jellinek@anl.gov (J.J.). Tel.: (630) 252-3463.
*E-mail: kbowen@jhu.edu (K.H.B.).

ORCID

Kit H. Bowen, Jr.: 0000-0002-2858-6352
Julius Jellinek: 0000-0001-8241-3623

Notes

The authors declare no competing financial interest.

ACKNOWLEDGMENTS

We thank Lai-Sheng Wang for permission to use parts of his published PES data on Al_4^- and Al_5^-. The experimental part of this material is based upon work supported by the Air Force Office of Scientific Research (AFOSR) under grant number FA9550-15-1-0259 (K.H.B.). The theoretical work at Argonne was supported by the Office of Basic Energy Sciences, Division of Chemical Sciences, Geosciences and Biosciences, U.S. Department of Energy under Contract No. DE-AC02-06CH11357 (J.J.).

REFERENCES

(1) Jena, P.; Sun, Q. Super Atomic Clusters: Design Rules and Potential for Building Blocks of Materials. *Chem. Rev.* **2018**, *118*, 5755–5870.
(2) *Metal Clusters and Nanoalloys: From Modeling to Applications*; Mariscal, M. M., Oviedo, O. A., Leiva, E. P. M., Eds.; Springer: New York, 2013.

DOI: 10.1021/acs.jpcc.8b06769
J. Phys. Chem. C 2019, 123, 7810–7817

(3) Acioli, P. H.; Jellinek, J. Electron Binding Energies of Anionic Magnesium Clusters and the Nonmetal-to-Metal Transition. *Phys. Rev. Lett.* **2002**, *89*, 213402 (1−4).
(4) Thomas, O. C.; Zheng, W.-J.; Xu, S.-J.; Bowen, K. H. Onset of Metallic Behavior in Magnesium Clusters. *Phys. Rev. Lett.* **2002**, *89*, 213403 (1−4).
(5) Jellinek, J.; Acioli, P. H. Magnesium Clusters: Structural and Electronic Properties and the Size-Induced Nonmetal-to-metal Transition. *J. Phys. Chem. A* **2002**, *106*, 10919−10925; *J. Phys. Chem. A* **2003**, *107*, 1670−1670.
(6) von Issendorff, B.; Cheshnovsky, O. Metal to Insulator Transition in Clusters. *Annu. Rev. Phys. Chem.* **2005**, *56*, 549−580.
(7) Ferrando, R.; Jellinek, J.; Johnston, R. L. Nanoalloys: From Theory to Applications of Alloy Clusters and Nanoparticles. *Chem. Rev.* **2008**, *108*, 845−910.
(8) *Nanoalloys: From Theory to Applications*, Faraday Discussions No. 138; RSC Publishing: Cambridge, 2008.
(9) *Nanoalloys: From Fundamentals to Emergent Applications*; Calvo, F., Ed.; Elsevier: Amsterdam, 2013.
(10) Lineberger, W. C. Once upon Anion: A Tale of Photodetachment. *Annu. Rev. Phys. Chem.* **2013**, *64*, 21−36.
(11) Jellinek, J.; Acioli, P. H. Computational Electron Spectroscopy of Gas Phase Metal Clusters. In *The Chemical Physics of Solid Surfaces*; Woodruff, D. P., Ed.; Elsevier: Amsterdam, 2007; Vol. *12*, pp 299−326.
(12) Akola, J.; Manninen, M.; Hakkinen, H.; Landman, U.; Li, X.; Wang, L.-S. Aluminum Cluster Anions: Photoelectron Spectroscopy and An Initio Simulations. *Phys. Rev. B: Condens. Matter Mater. Phys.* **2000**, *62*, 13216−13228.
(13) Acioli, P. H.; Jellinek, J. Theoretical Determination of Electron Binding Energy Spectra of Anionic Magnesium Clusters. *Eur. Phys. J. D* **2003**, *24*, 27−32.
(14) Jellinek, J.; Acioli, P. H.; Garcia-Rodeja, J.; Zheng, W.; Thomas, O. C.; Bowen, K. H., Jr. Mn^- Clusters: Size-Induced Transition To Half Metallicity. *Phys. Rev. B: Condens. Matter Mater. Phys.* **2006**, *74*, 153401 (1−4).
(15) Acioli, P. H.; Jellinek, J. Theoretical Analysis of Photoelectron Spectra of Pure and Mixed Metal Clusters: Disentangling Size, Structure and Composition Effects. *J. Phys. Chem. C* **2017**, *121*, 16665−16672.
(16) Jellinek, J.; Krissinel, E. B. NinAlm Alloy Clusters: Analysis of Structural Forms and Their Energy Ordering. *Chem. Phys. Lett.* **1996**, *258*, 283−292.
(17) Cui, L.-F.; Lin, Y.-C.; Sundholm, D.; Wang, L.-S. A Photoelectron Spectroscopic and Computational Study of Sodium Auride Clusters, $Na_nAu_n^-$ (n = 1−3). *J. Phys. Chem. A* **2007**, *111*, 7555−7561.
(18) Sobhy, M. A.; Reveles, J. U.; Gupta, U.; Khanna, S. N.; Castleman, A. W. Photoelectron Imaging and Theoretical Investigation of Bimetallic $Bi_{1-2}Ga_{0-2}^-$ and Pb_{1-4}^- Cluster Anions. *J. Chem. Phys.* **2009**, *130*, 054304 (1−9).
(19) Xie, H.; Li, X.; Zhao, L.; Qin, Z.; Wu, X.; Tang, Z.; Xing, X. Photoelectron Imaging and Theoretical Calculations of Bimetallic Clusters: $AgCu^-$, $AgCu_2^-$, and Ag_2Cu^-. *J. Phys. Chem. A* **2012**, *116*, 10365−10370.
(20) Zhang, X.; Gantefoer, G.; Bowen, K. H.; Alexandrova, A. The $PtAl^-$ and $PtAl_2^-$ Anions: Theoretical and Photoelectron Spectroscopic Characterization. *J. Chem. Phys.* **2014**, *140*, 164316 (1−4).
(21) Deng, X.-J.; Kong, X.-Y.; Xu, X.-L.; Xu, H.-G. Structural and Magnetic Properties of $CoGe_n^-$ (n = 2−11) Clusters: Photoelectron Spectroscopy and Density Functional Calculations. *ChemPhysChem* **2015**, *15*, 3987−3993.
(22) Buendia, F.; Beltran, M. R.; Zhang, X.; Liu, G.; Buytendyk, A.; Bowen, K. *Ab Initio* and Anion Photoelectron Study of Au_nRh_m (n = 1−7, m = 1−2) Clusters. *Phys. Chem. Chem. Phys.* **2015**, *17*, 28219−28227.
(23) Jian, T.; Lopez, G. V.; Wang, L.-S. Photoelectron Spectroscopy of $BiAu^-$ and $BiBO^-$: Further Evidence of the Analogy between Au and Boronyl. *J. Phys. Chem. B* **2016**, *120*, 1635−1640.
(24) Khetrapal, N. S.; Jian, T.; Lopez, G. V.; Pande, S.; Wang, L.-S.; Zeng, X. C. Probing the Structural Evolution of Gold−Aluminum Bimetallic Clusters ($Au_2Al_n^-$, n = 3−11) Using Photoelectron Spectroscopy and Theoretical Calculations. *J. Phys. Chem. C* **2017**, *121*, 18234−18243.
(25) Li, X.; Grubisic, A.; Stokes, S. T.; Cordes, J.; Gantefoer, G. F.; Bowen, K. H.; Kiran, B.; Willis, M.; Jena, P.; Burgert, R.; et al. Unexpected Stability of Al_4H_6: A Borane Analog? *Science* **2007**, *315*, 356−358.
(26) Zhang, X.; Wang, Y.; Wang, H.; Lim, A.; Gantefoer, G.; Bowen, K. H.; Reveles, J. U.; Khanna, S. N. On the Existence of Designer Magnetic Superatoms. *J. Am. Chem. Soc.* **2013**, *135*, 4856−4861.
(27) Ho, J.; Ervin, K. M.; Lineberger, W. C. Photoelectron Spectroscopy of Metal Cluster Anions: Cu_n^-, Ag_n^-, and Au_n^-. *J. Chem. Phys.* **1990**, *93*, 6987−7002.
(28) Becke, A. D. Density-functional Exchange-energy Approximation with Correct Asymptotic Behavior. *Phys. Rev. A: At., Mol., Opt. Phys.* **1988**, *38*, 3098−3100.
(29) Perdew, J. P. Density-Functional Approximation for the Correlation Energy of the Inhomogeneous Electron Gas. *Phys. Rev. B: Condens. Matter Mater. Phys.* **1986**, *33*, 8822−8824.
(30) Andrae, D.; Haeussermann, U.; Dolg, M.; Stoll, H.; Preuss, H. Energy-Adjusted *Ab Initio* Pseudopotentials for the Second and Third Row Transition Elements. *Theor. Chem. Acc.* **1990**, *77*, 123−141.
(31) Frisch, M. J.; Trucks, G. W.; Schlegel, H. B.; Scuseria, G. E.; Robb, M. A.; Cheeseman, J. R.; Montgomery, J. A., Jr.; Vreven, T.; Kudin, K. N.; Burant, J. C.; et al. *Gaussian 03*, Revision C.02; Gaussian, Inc.: Wallingford CT, 2004.
(32) Jellinek, J.; Acioli, P. H. Converting Kohn−Sham Eigenenergies into Electron Binding Energies. *J. Chem. Phys.* **2003**, *118*, 7783−7796.
(33) Li, X.; Wu, H.; Wang, X.-B.; Wang, L.-S. s-p Hybridization and Electron Shell Structures in Aluminum Clusters: A Photoelectron Spectroscopy Study. *Phys. Rev. Lett.* **1998**, *81*, 1909−1912.
(34) Melko, J. J.; Castleman, A. W., Jr. Photoelectron Imaging of Small Aluminum Clusters: Quantifying s−p Hybridization. *Phys. Chem. Chem. Phys.* **2013**, *15*, 3173−3178.
(35) Feynman, R. P. There's Plenty of Room at the Bottom. *Eng. Sci.* **1960**, *23*, 22−36.

DOI: 10.1021/acs.jpcc.8b06769
J. Phys. Chem. C 2019, 123, 7810−7817